Applied Thermal Engineering 180 (2020) 115889

Contents lists available at ScienceDirect

Applied Thermal Engineering

journal homepage: www.elsevier.com/locate/apthermeng

Experimental analysis of a micro-scale organic Rankine cycle system retrofitted to operate in grid-connected mode

Muhammad Usman[a,b,*], Muhammad Imran[c,d], Fredrik Haglind[c], Apostolos Pesyridis[a], Byung-Sik Park[e]

[a] Centre of Advanced Powertrain and Fuels, Department of Mechanical, Aerospace, & Civil Engineering, Brunel University London, Uxbridge, UB8 3PH London, United Kingdom
[b] Entropea Labs Limited, Arquen House, 4-6 Spicer Street, St. Albans, Hertfordshire, England AL3 4PQ, United Kingdom
[c] Section of Thermal Energy (TES), Department of Mechanical Engineering, Technical University of Denmark, Nils Koppels Allé 403, 2800 Kongens Lyngby, Denmark
[d] School of Engineering and Applied Science, Aston University, B4 7ET Birmingham, United Kingdom
[e] Energy Network Laboratory, Korea Institute of Energy Research (KIER), 152 Gajeong-ro, Yuseong-gu, 34129 Daejeon, Republic of Korea

HIGHLIGHTS

- An off-grid 1kWe class ORC was retrofitted to operate in a grid-connected mode.
- Experimental comparison of performance curve is compared for both operational modes.
- Net thermal to electric conversion efficiency 7.36% in grid-connected mode.
- Maximum electric power generation was 1.162 kW (gross) and 0.967 kW (net)
- Same machine can perform differently when control schemes are different.

ARTICLE INFO

Keywords:
Organic Rankine cycle
Grid-connected mode
Off-grid mode
R245fa
Scroll expander
Waste heat recovery

ABSTRACT

This work presents the retrofitting of a micro-scale organic Rankine cycle system originally designed for off-grid operation, modified to operate in grid-connected mode. Quantitative and qualitative performance comparisons of the grid-connected and off-grid connected organic Rankine cycle system are made based on experimental data of an organic Rankine cycle test rig. The operating strategies of the two systems are discussed in detail. The organic Rankine cycle test rig has a nominal power output of 1 kW with R245fa as the working fluid, a scroll expander as the expansion machine and steam as the heat source. Initially, the experiments were performed in off-grid operation mode with a self-excited alternating current generator. Subsequently, the organic Rankine cycle test rig was retrofitted for grid-connected mode, replacing the alternating current generator with an induction motor, regenerative variable frequency drive and grid connection. The rig modification was carefully done in such a way that the expander rotational speed was not fixed by the grid frequency, offering an additional control parameter for operational control optimisation. The modified system is able to supply 1.162 kW of gross electric power to the grid while a net electric output of 0.967 kW is measured. The same system is able to generate 1.016 kW (gross) and 0.838 kW (net) electric output in grid-connected mode. The net thermal-to-electric conversion efficiency at peak power generation is 7.36% and 4.66% in grid-connected and off-grid operating mode, respectively.

1. Introduction

The global community is striving to reduce emissions and limit global warming below 2 °C as agreed in the 2015 United Nations Climate Change Conference [1]. The European Union (EU) has also adopted a 20-20-20 emission reduction policy, which involves reducing emissions by 20%, shifting energy dependency on renewable sources by at least 20%, and improving the conversion efficiencies of already established systems by 20% [2]. New ideas are necessary in order to fulfil the future energy requirements of the ever-increasing population

* Corresponding author at: Centre of Advanced Powertrain and Fuels, Department of Mechanical, Aerospace, & Civil Engineering, Brunel University London, Uxbridge, UB8 3PH London, United Kingdom.
E-mail address: usman7@live.com (M. Usman).

https://doi.org/10.1016/j.applthermaleng.2020.115889
Received 28 March 2020; Received in revised form 24 July 2020; Accepted 11 August 2020
Available online 17 August 2020

Nomenclature

Parameters and Acronyms

AC	Alternating current
BWR	Back work ratio
BOP	Balance of plant
CHP	Combined Heat & Power
cRIO	Compact Reconfigurable Input Output
DC	Direct current, A
FS	Full scale
h	Enthalpy, kJ/kg
LNG	Liquid Natural Gas
ORC	Organic Rankine Cycle
$\dot{m}$	Mass flow rate, kg/s
NPSHA	Net positive suction head available, m H2O
P	Pressure, bar
PR	Pressure ratio
$\dot{Q}$	Heat Transfer Rate, kW
SPST	Single Push Single Throw
T	Temperature, °C
VFD	Variable frequency drive
W	Power output, kW

Greek letters

η	Efficiency

Subscripts

in	Input to the working fluid
wf	Working fluid
evap	Evaporator
fec	Fluid work potential to electric conversion
isc	Isentropic
th	Thermal
trn	watt transducer
net	Net
em	Electro-mechanical
exp	Expander

without violating the emission targets.

Organic Rankine Cycle (ORC) based, heat-to-power conversion systems, is being considered as a viable solution to increase the conversion efficiency by recovering waste heat energy and providing flexibility to adopt renewable energy sources [3]. ORC systems are being investigated for internal combustion engine-based prime movers for the heat to electric conversion in the power and transportation sectors [4]. Another promising application of ORC technology is the development of industrial waste heat-to-electric power conversion [5]. Recent studies on waste heat recovery in energy-intensive industries revealed that up to about 20,000 GWh of thermal energy can be recovered by the use of ORC technology and 7.6 M ton of CO_2 can be saved in the EU alone [6].

ORC power systems can be classified by two major criteria: heat source/cycle temperature and power output. If the cycle maximum temperature is above 250 °C, the system is classified as high-temperature, for a medium-temperature system the maximum cycle temperature is in the range of 150–250 °C, and below 150 °C it is referred to as a low-temperature system. Power systems below the output of 3 kW are referred as micro, 3 kW to 50 kW are mini, 50–500 kW are small, 0.5 MW to 5 MW are medium, and systems capable of power output larger than 5 MW are large-scale systems [7]. Statistical analysis reveals that low-grade waste heat accounts for 50% or more of the total heat generated in industry [8,9], thus making the low-temperature ORC technology of prime importance for energy recovery. The adaptability of an ORC unit to different heat sources, unmanned operation, low maintenance, minimal interference with the operator's main task and environment-friendly operation have contributed to increasing the research and development efforts of low-temperature ORC systems [10]. The ORC system can be integrated to heating, cooling, and desalination as well [11]. Despite the promising capabilities of the ORC technology, commercial small-scale systems for low-temperature application are still at a fairly low technology readiness level [12].

The complex techno-economics, lower efficiencies due to the smaller temperature difference in sink and source, non-availability of suitable components and limited availability of data from experimental test rigs have contributed to a slow maturity of the technology, especially for the low-temperature based mini and micro-scale systems.

Many works have contributed to ORC technology development, bringing it a step closer to commercialisation [13]. Working fluid selection is considered one of the key parameters for the success of an ORC system. Walraven et al. [14] reported that the choice of optimal working fluid is dependent on the heat source and sink conditions. Saleh et al. [15] suggested that based on the thermodynamic efficiency for low-temperature ORC systems, R236ea, R245ca, R245fa and R600 are the suitable options. Xu et al. [16] reported that fluids like R245fa can be used for a wide variety of heat source conditions in a low-temperature operational regime. In a recent work, Muhammad et al. [17] suggested that R1233ZD can be a potential replacement for R245fa.

The selection of the expansion machine is another topic of research interest in the ORC field. Expansion machines are categorised into two broad categories: positive displacement (volumetric) expanders and velocity based expanders (turbines). The volumetric machines are suitable for micro-scale application due to low cost, simplicity, low rotational speeds and tolerance of two-phase flows [18–20]. Qui et al. [21] suggested that for ORC systems of size 1–10 kW, scroll and vane type expanders are suitable choices. Multi-vane machines are cheaper solutions given that their sealing problems have been resolved [22]. Chang et al. [23] tested an open drive scroll expander to work as an expander yielding a maximum of 73% isentropic efficiency. Declaye et al. [24] reported that oil-free expanders simplify the ORC system design for a 2.1 kW power output.

Experimental testing of low-temperature systems has also been reported for various configurations and equipment combinations. Pei et al. [25] discussed the performance of a 3.75 kW scale ORC test rig using R123 as the working fluid. The system achieved 1 kW shaft power and 6.8% cycle efficiency with a 70 °C temperature difference. Another R123 based ORC test rig was tested by Miao et al. [26] with a heat source temperature of 160 °C, and 5.12% thermal output was reported while delivering 3.25 kW shaft power. Farrokhi et al. [27] tested a R601a based ORC system in a combined heat and power (CHP) configuration and reported 77.4 W of electrical power output with 1.66% efficiency. Wang et al. [28] reported a regenerative ORC based on R245fa and reported a thermal efficiency of 3.67%. Yamada et al. [29] reported a micro-scale ORC with 5 W power output with a heat source temperature below 100 °C. Pethurajan et al. [30] reported an experimental study of a multi-expander configuration for a micro-scale ORC operating with R245fa and maximum power output of 3.3 kW. These experimental studies mainly focused on standalone systems, and none of them considered a grid-connected ORC system. In addition, very few of the experimental works considering ORC systems in the micro and mini-scales address the ability of the ORC system to generate electricity.

Usman et al. [31] discussed the ability of a micro ORC to yield a net electrical output in an off-grid configuration using steam as a heat source without an intermediate heat transfer loop. Operational control

optimisation was also presented for the same test rig [32] for off-grid installation. A database of the experimental studies in the area of ORC systems [33] indicates that the experimental performance of the ORC systems is always investigated using a resistive load, that is, the system can be considered as an off-grid or standalone system. The literature review further suggests that there are very few studies presenting an experimental investigation of a micro/mini-scale grid-connected ORC system and performance comparison with a corresponding off-grid ORC system. To the best of the authors' knowledge, until now, only Feng et al. [34] compared the operation of a 10 kW ORC machine in off-grid and grid-connected operation. However, in grid connection operation, the expander rotational speed was fixed and was governed by grid frequency. The need for insight into the net power output performance curve for both operational schemes, also when employing a variable speed expander, justifies yet another paper targeting the comparison of off-grid and grid-connected modes.

Due to widespread nature of the heat source, the power produced by the ORC system can be categorized as distributive power generation. Depending upon the size of the ORC system and local rules for grid connection, an ORC system can be connected to grid.

The objective of the present paper is to provide the quantitative and qualitative performance comparison of the grid-connected and off-grid connected ORC system based on experimental data of a 1 kWe ORC test rig. The test rig employs a robust grid connection configuration where the expander rotational speed is not fixed by the grid frequency, but rather can be adjusted to operate close to the best performance point. The additional control parameter allows a larger control envelope to optimise an operational control scheme. The components and configuration of additional components for the retrofitting of the ORC system to convert it from off-grid mode to grid-connected mode are presented. The paper also presents a comparison of cycle thermodynamic parameters for peak power output in both grid-connected and off-grid operation along with the explanation of differences between the performance curves.

The background of the research work and literature review are presented in Section 1 of the paper. The research methodology is described in Section 2. The results and discussion are presented in Section 3. Finally, the concluding remarks are presented in Section 4.

2. Material & methods

The temperature-entropy (T-s) diagram of the ORC system and corresponding thermodynamic states are shown in Fig. 1. The process 1-2 represents the non-isentropic process of the pump, 2-3 is the preheating of the working fluid, the process 3-4 represents the evaporation process and the bulk of heat transfer from the heat source (steam) to the working fluid, and the process 4-5 represents the superheating to avoid any droplets in the expander. The process 5–6 represents the real gas expansion in the expander, and 6-1 represents the heat rejection by the condenser.

The ORC thermodynamic design and balance of plant (BOP) was already fixed and remains mostly as documented in our previous work [31]. The schematic of the experimental test rig, both with off-grid and grid-connected mode (shown in each block), is presented in Fig. 2. The system was initially tested with the off-grid configuration, and then the off-grid block as mentioned in the schematic was replaced with the grid-connected block. The replacement of the components (generator/motor) was required to ensure optimal matching with the grid and flexibility to operate and control the system. An induction motor was connected with the expander with the help of a magnetic coupling.

The experimental test rig is shown in Fig. 3, and the off-grid operation mode as a self-excited alternating current (AC) generator can be seen. The retrofitting requires changing the components after the expander, and the rest of the components are the same for both operational modes. The components required for the off-grid testing and grid-connected mode testing are shown in Fig. 4. For the grid-connected mode, the overall footprint of the rig was unaltered (0.74 m length × 2 m width × 2 m height).

ORC systems equipped with volumetric expansion machines can be easily connected with the grid, as the expansion machine frequency is often close to the grid frequency. In this case, a common practice is to use the induction motor which, when powered by the grid, will make the expander rotate close to the synchronous speed (around grid frequency) with a difference of a slip [35].

An induction motor consists of two assemblies: a stator and a rotor. The interaction of the currents flowing in the rotor bars and the stators' rotating magnetic field generates a torque. In an actual operation, the rotor speed always lags behind the magnetic field speed, allowing the rotor bars to cut magnetic lines of force and produce useful torque. Slip is defined as the difference between the synchronous speed of the magnetic field and the shaft rotating speed.

The work done by the expander is converted to additional torque, which will make the rotor of the motor rotate at a higher speed than the synchronous speed, causing current reversal and an electric power generation and supply to the grid. For the current system, it was necessary to vary the synchronous speed in order to be able to study the expander operation at various rotational speeds. This was achieved by a regenerative variable frequency drive (VFD) being implemented between the motor and grid, thus allowing the experiment to be performed at any rotational speed of the expander. The VFD was controlled with a Compact Reconfigurable Input Output (cRIO)-based controller using analogue output. Initially, the signal from the regenerative VFD fixes the expander speed (grid frequency). The induction motor operates in motor mode, as the rotor speed is lower than the speed of the magnetic field. As a result, the expander contributes to the pumping action. When the pressure difference is large enough, the expander starts exerting additional torque, and the rotor speed exceeds the speed of the magnetic field. Thus, the motor operation of the induction motor smoothly turns into generator mode. The technical details of the equipment are listed in Table 1.

The REFPROP software [36] was used to evaluate the thermodynamic states with reference to the temperature and the pressure sensor readings. The heat transfer rate to the working fluid was calculated as follows:

$$\dot{Q}_{in} = \dot{m}_{wf}(h_{evap,out} - h_{evap,in}) \quad (1)$$

Expander isentropic efficiency was calculated as follows (with reference to Fig. 1 stations):

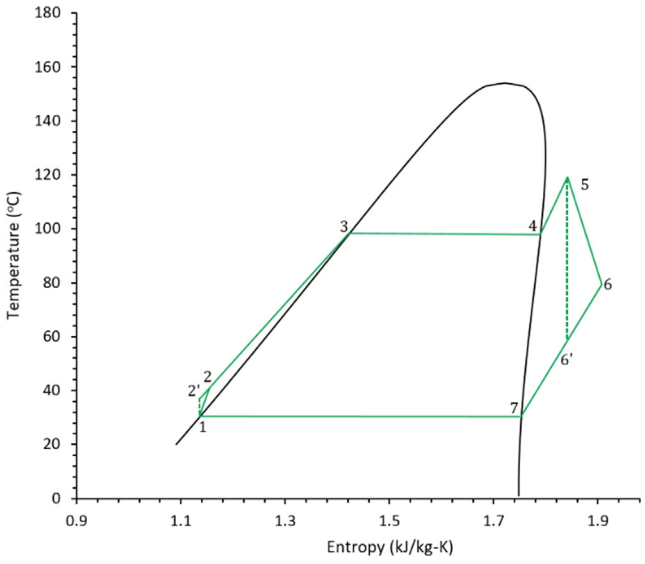

Fig. 1. Temperature-Entropy (Ts) diagram of the ORC system.

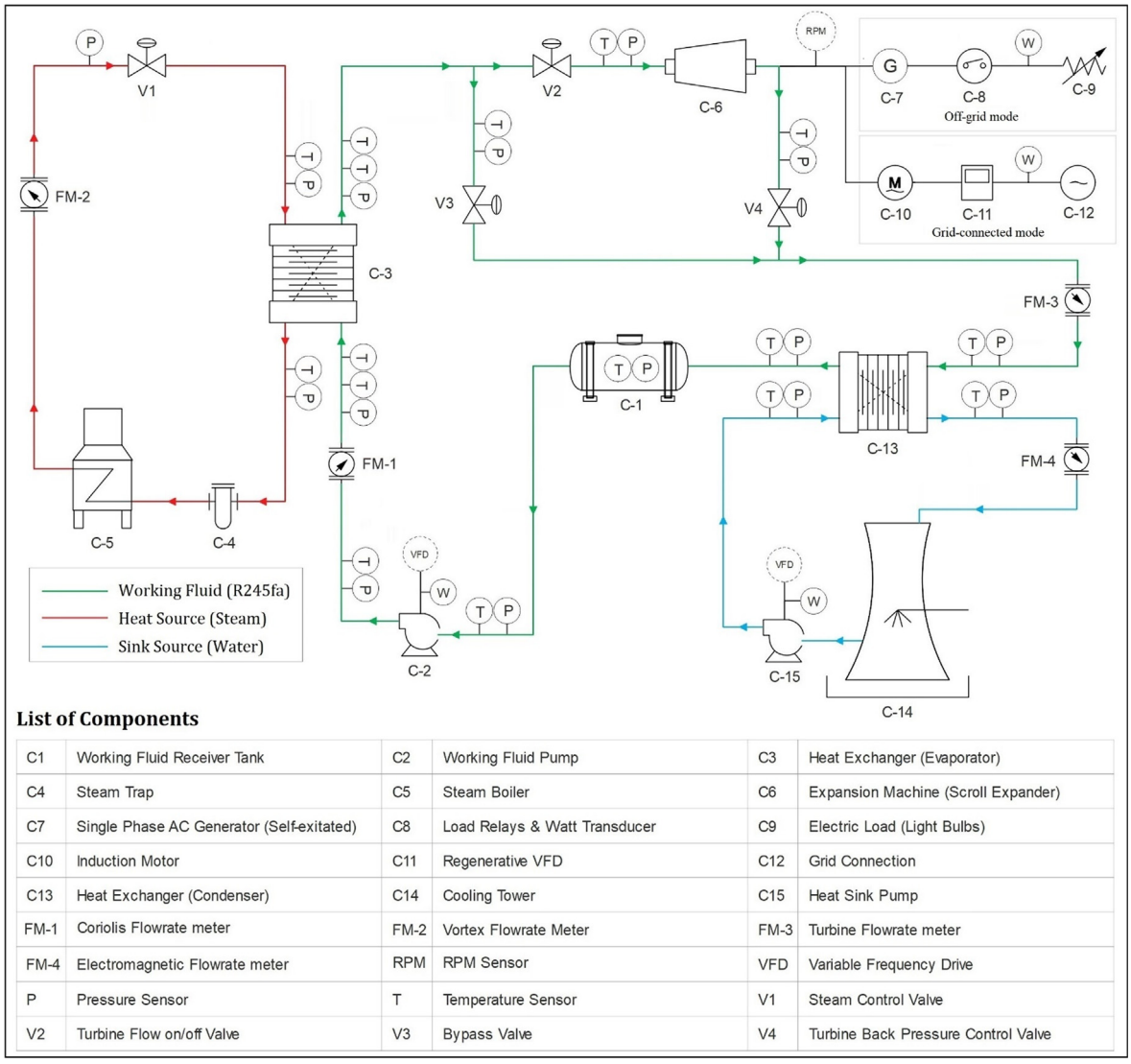

List of Components

C1	Working Fluid Receiver Tank	C2	Working Fluid Pump	C3	Heat Exchanger (Evaporator)
C4	Steam Trap	C5	Steam Boiler	C6	Expansion Machine (Scroll Expander)
C7	Single Phase AC Generator (Self-exitated)	C8	Load Relays & Watt Transducer	C9	Electric Load (Light Bulbs)
C10	Induction Motor	C11	Regenerative VFD	C12	Grid Connection
C13	Heat Exchanger (Condenser)	C14	Cooling Tower	C15	Heat Sink Pump
FM-1	Coriolis Flowrate meter	FM-2	Vortex Flowrate Meter	FM-3	Turbine Flowrate meter
FM-4	Electromagnetic Flowrate meter	RPM	RPM Sensor	VFD	Variable Frequency Drive
P	Pressure Sensor	T	Temperature Sensor	V1	Steam Control Valve
V2	Turbine Flow on/off Valve	V3	Bypass Valve	V4	Turbine Back Pressure Control Valve

Fig. 2. The schematic of the ORC test rig (blocks show off-grid and grid-connected modes).

$$\eta_{\text{isc}} = \frac{h_5 - h_6}{h_5 - h_{6'}} \times 100 \tag{2}$$

The net power output was calculated as follows:

$$\dot{W}_{\text{net}} = \dot{W}_{\text{exp}} - \dot{W}_{\text{pu}} \tag{3}$$

The thermal efficiency was evaluated as follows:

$$\eta_{th} = \frac{\dot{W}_{\text{exp}}}{\dot{Q}_{\text{in}}} \times 100 \tag{4}$$

The net thermal efficiency of the ORC system was computed as follows:

$$\eta_{\text{net}} = \frac{\dot{W}_{\text{net}}}{\dot{Q}_{\text{in}}} \times 100 \tag{5}$$

The expander pressure ratio is given by

$$PR = \frac{P_{\text{in,exp}}}{P_{\text{out,exp}}} \tag{6}$$

Equation (7) calculates electro-mechanical efficiency accounting for the mechanical losses in the expander, coupling, and generator and the electrical conversion losses in the motor/generator along with power electronics

$$\eta_{\text{em}} = \frac{\dot{W}_{\text{trn}}}{\dot{m}_{\text{wf}}(h_5 - h_6)} \times 100 \tag{7}$$

$\dot{W}_{\text{trn}}$ is electric power output of generator measure by watt transducer. Fluid work potential to electrical conversion efficiency, which accounts for all losses in the process of conversion of fluid power to electric power, is given by

$$\eta_{\text{fec}} = \eta_{\text{em}} \cdot \eta_{\text{isc}} \tag{8}$$

The back work ratio for the system is given by

$$BWR = \frac{\dot{W}_{\text{pu}}}{\dot{W}_{\text{trn}}} \tag{9}$$

The rig operation in the grid-connected mode is different compared to the off-grid system operation in a number of ways. The start-up was initiated with the circulation of the working fluid in the evaporator and gradual increase in heat source flow, while the expander inlet valve was initially closed and the bypass valve was completely open. Upon the detection of a superheated state of the working fluid, the expander inlet valve was opened to 100%, and expander rotation was started in motoring mode; this enabled a faster start-up and warm-up of the machine before pressurisation. The bypass valve was closed gradually, the system was pressurised, and the motoring operation was converted into generation.

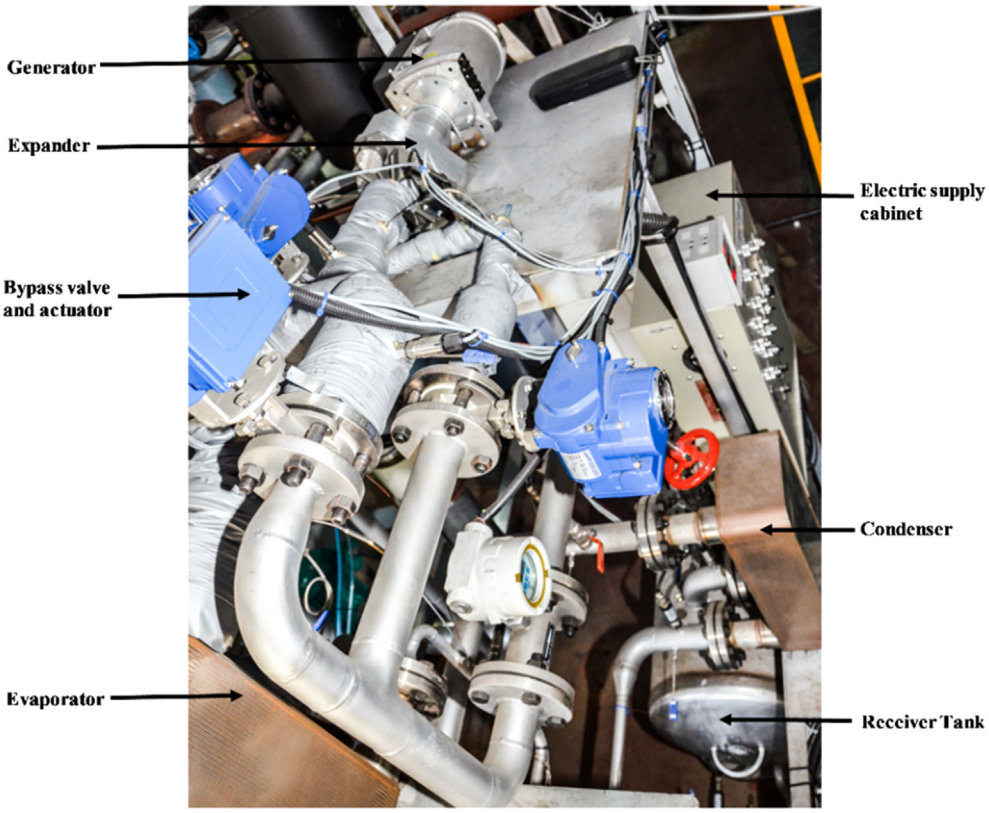

Fig. 3. ORC test rig after fabrication (off-grid mode).

The VFD switches automatically to regeneration mode and starts the electric power supply to the grid without involving complex power electronics. The increase in pump speed increased the pressurisation, thus resulting in a larger pressure ratio. The higher-pressure ratio resulted in larger torque and increased power output.

The expander rotational speed was traversed between 1800 RPM and 3600 RPM. Different operational speeds can alter the choking phenomena in the expander and lead to a change in pressure ratio even at fixed pump speed. The learning outcomes of multispeed operation expander operations include cautious/hazardous operation if the expander speed is too low. The low rotational speed of the expander caused a high-pressure difference at a smaller mass flow rate, leading the pump to operate outside of its design envelope and causing flow reversals. Another caution for low speed and high power operation of the expander is that it exerts very high torque leading to high mechanical stresses and slippage in the magnetic coupling. Prolonged operation in such state where speed is low, but power is high, will also exert a larger current in the motor coils leading to failure. Overcurrent protection was provided by the regenerative VFD which would shut off the power transfer, but this can result in expander runaway which, if not contained by automatic fast-acting valves, may lead to mechanical damage of the expander. Both systems were operated following a heat source operating scheme instead of following electric load. The maximum operational performance of the ORC was limited by complete exploitation of the heat source, maximum pressure, or pump operational envelope.

Data acquisition and control was performed by National Instrumentation cRIO-9074 with 8 slot integrated 400 MHz real-time controller. National Instruments C-Series input output modules were used to measure thermocouple, RTD, pressure transducers, power

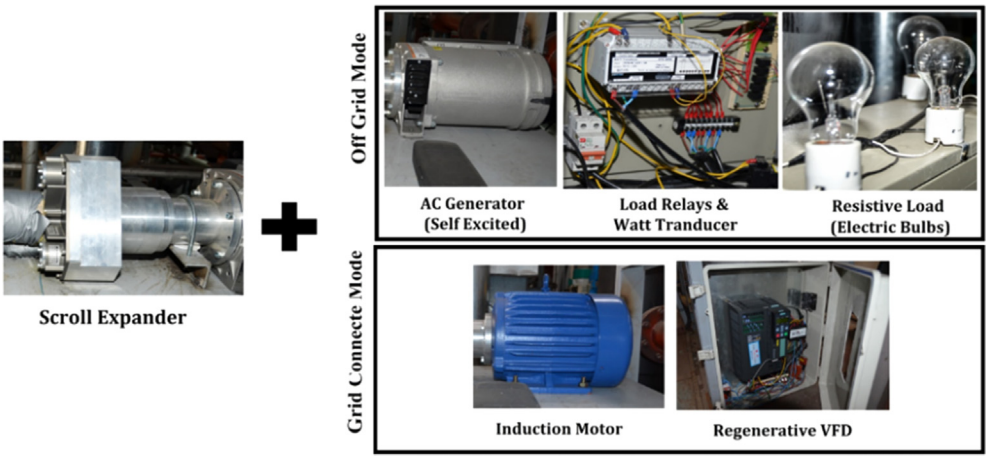

Fig. 4. Components in each block for off-grid and grid-connected operation.

Table 1
Details of the individual components of the ORC test rig.

Equipment	Details	
Evaporator	Brazed plate heat exchanger (Janghan Engineers, Inc.) 60 plates, heat transfer area = 6.5 m^2	
Condenser	Brazed plate heat exchanger (Janghan Engineers, Inc.) 50 plates, heat transfer area = 5.38 m^2	
Feed pump	Screw type pump (Tuthill pump company) Displacement of 2.6 m l/rev, magnetic coupling linked to 0.75 kW 3-phase 380 V motor.	
Generator	*Off-grid mode:*	Single-phase 120VAC generator with full wave rectifier and capacitor for self-excitation to enable off-grid operation (Wanco, Inc.), directly coupled with expander by magnetic coupling, 2.4 kW nominal output
	Grid-connected mode:	Induction motor (LG), 2.2 kWe nominal, 2 pole 380 VAC
Electric load connection	*Off-grid mode:*	Electric Bulbs of various power ratings were connected to the generator using single push single throw (SPST) type relays. Bulbs for 110 V were used in different power rating combinations. 200 W, 100 W, 60 W, and 30 W watt bulbs were used to obtain various steps of the resistive load connected to the generator
	Grid-connected mode:	Via regenerative variable frequency drive (Siemens), G120 inverter with a PM250 power unit
Heat source	LNG based boiler with a steam generation capacity of 500 kg/h maximum	
Expander	Scroll type expander (Air squared Inc.) model E15H22N4.25, displacement = 12 cc/rev, design expansion ratio = 3.5:1, oil free, 1 kW nominal output	
Valves	Butterfly valves and globe valve (actuator controlled with position feedback)	
Flow rate meters	Working fluid	Coriolis flow meter (KOMETER), Tolerance 0.2%+/- FS, 0–555.6 g/s range
	Cooling water	Electro-magnetic flow meter (KOMETER), Tolerance = ± 0.5% FS, 0–10 m^3/h range
RPM measurement	Multi-meter based Tachometer probe (compact instruments) range 0–6000RPM, tolerance = ± 0.5% FS	
Temperature measurement	T -type thermocouples for temperature measurement RTD (PT100) for evaporator and expander inlet/exit	
Power measurement	Watt Transducers, accuracy ± 0.25% full scale, (3 W max error in all operational range)	
Pressure Transduces	Pressure Transducers of 0–16 bar, (Huba Control) tolerance = ± 0.5% full scale	
Data Acquisition	National Instruments - cRIO 9074 with 8 slots integrated controller, National Instruments I/O C-series model and LabVIEW software	

readings, flow rate measurements, control valve position and generator speed.

Electric load relays, pump variable frequency drive and valve control were the outputs of control system. Labview Real software was used to implement control logic and data acquisition for the test bed. The uncertainty of the measuring instruments is shown in Table 2.

3. Results & discussion

At first the off-grid experiments were performed, and part of the results of the off-grid system were reported in our previous work [31]. The ORC test rig was retrofitted with components that were required for grid-connected operation, and experiments were performed. All efforts were put into achieving the heat source and sink conditions closer to the experimental data acquired with the off-grid operation to ensure a fair comparison. However, the cooling water temperature was not exactly the same. The limitation was imposed because the cooling water was supplied by an over sized cooling tower suppling chilled water to various utilities. The cooling water temperature was impacted by local weather conditions and thermal inertia of cooling loop. Despite both experiments being performed in same winter months, it was not possible to achieve exact same temperature. Table 3 presents a comparison of the grid-connected mode and off-grid mode at the peak power output operating point.

The grid-connected system was able to achieve a higher power output compared with the maximum power output of the off-grid system. The ORC thermal efficiency at the maximum power output was η_{th} = 8.85% and η_{net} = 7.36%. The maximum thermal efficiency in grid-connected operation was at part-load conditions, where the pressure ratio was 9.72 and the thermal efficiency was η_{th} = 10.2% and η_{net} = 8.68%.

The reasons for the higher power output in grid-connected mode include, more efficient electro-mechanical systems, better equipment operating point match with peak performance, and a higher pressure ratio achieved in the grid-connected system. The comparison reveals that sink supply temperature to condenser was lower and the mass flow rate was higher in off-grid mode; the condensing pressure was slightly higher if compared with the grid-connected operation. The higher condensing pressure resulted in a smaller pressure ratio across the expander even with higher evaporator pressure in off-grid operation. The higher condensing pressure is indicative of either a small quantity of non-condensing gasses which may be present in the system or a drop in performance (effectiveness) of the heat exchanger which may occur under larger heat load, which was the case in off-grid operation. Fig. 5 presents the gross power output measured for both the grid-connected and the off-grid scheme.

Net electrical power output calculated by Eq. (3) has also been plotted on the same scale. Second-order polynomials were plotted for all data as trend lines for projections around plotted data points. The trend for the off-grid system is acquired from the experiments described in Ref. [31] and compared with grid-connected operation. It is notable that at peak operation, both net and gross power output are higher for grid-connected operation.

The parabolic trend is far more pronounced in off-grid operation, while the grid-connected system has a trend closer to a linear relation with the pressure ratio. Another feature of the results suggests that at the same pressure ratio, the off-grid system can yield higher power output, but the trend also suggests that this will be reversed if the pressure ratio is above 11.3. The decrease in the net power is attributed to the over expansion losses of the expander.

Fig. 6 presents the thermal efficiency trend and pressure ratio for both grid-connected and off-grid operation as evaluated by Eq. (4) and Eq. (5). The parabolic trends with respect to the pressure ratio are in agreement with the generic cycle efficiency trend discussed in a

Table 2
Uncertainty of the measuring instruments.

Equipment	Company/Model	Uncertainty
Pressure transducers	Huba/510 series	± 0.50%
Thermocouples	Omega/K type	± 0.39 °C
Coriolis flow meter	KOMETER/ KMS-2000	± 0.20%
Turbine flow meter	KOMETER/ KTR-550	± 0.50%
Electromagnetic flow meter	KOMETER/ KTM-800	± 0.50%
Watt transducers	Lightstar/NA	± 0.25%
Tachometer	CA Instrument/A2108 series	± 0.50%

Table 3
Comparison of operating points at the maximum power output.

Component location	Thermodynamic state parameters					
	Peak operation point (Grid-connected mode)			Peak operation point (off-Grid mode)		
	T (°C)	P (bar)	h (kJ/kg)	T (°C)	P (bar)	h (kJ/kg)
Evaporator inlet (R245fa)	15.8	11.4	220.7	8.8	12.2	211.7
Evaporator outlet (R245fa)	128.0	11.4	511.9	132.2	12.1	515.6
Expander inlet	120.3	11.4	502.5	127.2	12.1	509.6
Expander outlet	71.1	0.9	468.1	84.2	1.1	480.5
Condenser inlet (R245fa)	58.9	0.9	467.8	71.1	1.1	467.7
Condenser outlet (R245fa)	14.7	0.9	210.3	9.4	1.1	212.1
Evaporator inlet (steam)	130.2	2.7	2720.4	135.4	3.1	2728.1
Evaporator outlet (steam)	97.0	2.6	406.6	12.9	2.9	54.5
Condenser inlet (chilled water)	9.1	1.3	38.7	4.9	1.3	20.7
Condenser outlet (chilled water)	15.4	1.3	64.7	7.2	1.3	30.4
ORC performance system data						
Expansion pressure ratio	12.09			10.81		
Mass flow rate of working fluid (g/s)	45.11			59.23		
Mass flow rate of chilled water (kg/s)	0.5			1.56		
Expander speed (RPM)	3499			3521		
Pump speed (RPM)	1799			1600		
Expander isentropic efficiency (%)	67.14			58.18		
Heat input rate to working fluid (kW)	13.14			18.00		
Electric generator power output (W)	1162.2			1016		
Electric power consumed in pumping (W)	195.3			178		
ORC system net power output (W)	966.9			838		
ORC thermal efficiency (%)	8.85			5.64		
ORC net thermal efficiency (%)	7.36			4.66		

previous study [24]. The grid-connected system has a better efficiency primarily due to smaller electro-mechanical losses. It can also be observed that the difference between net and gross efficiency is larger for grid-connected operation. The off-grid system has lower thermal efficiency, specifically for pressure ratios above 7.5.

Fig. 7 presents the variation in expander isentropic efficiency for the grid-connected and the off-grid system. Interestingly, the expander was the same in both cases, and the measurements used for the expander isentropic efficiency calculations were based on expander inlet and outlet working fluid conditions as detailed by Eq. (2), but the results are still significantly different at the same expansion ratio. The grid-connected systems represent a generic scroll machine efficiency parabolic curve where there is a peak efficiency at a certain pressure ratio, and before and after this peak operating point, the efficiency drops due to under and over expansion losses [24,37,38]. However, the off-grid performance represents the second half of the parabola only, and thus a decrease in expander isentropic efficiency was measured with the increasing pressure ratio.

A similar trend in the difference of isentropic efficiency for off-grid and grid-connected operation can also be extracted from the results presented in Ref. [39] where isentropic efficiency was plotted with respect to the heat input to the system. The rationale for the phenomenon is that although the expander is the same, this difference in efficiency is caused by the fact that, even at comparable expansion ratios, the absolute inlet pressure and temperature values are different. The leakage losses in the expansion machine are not only dependent on the

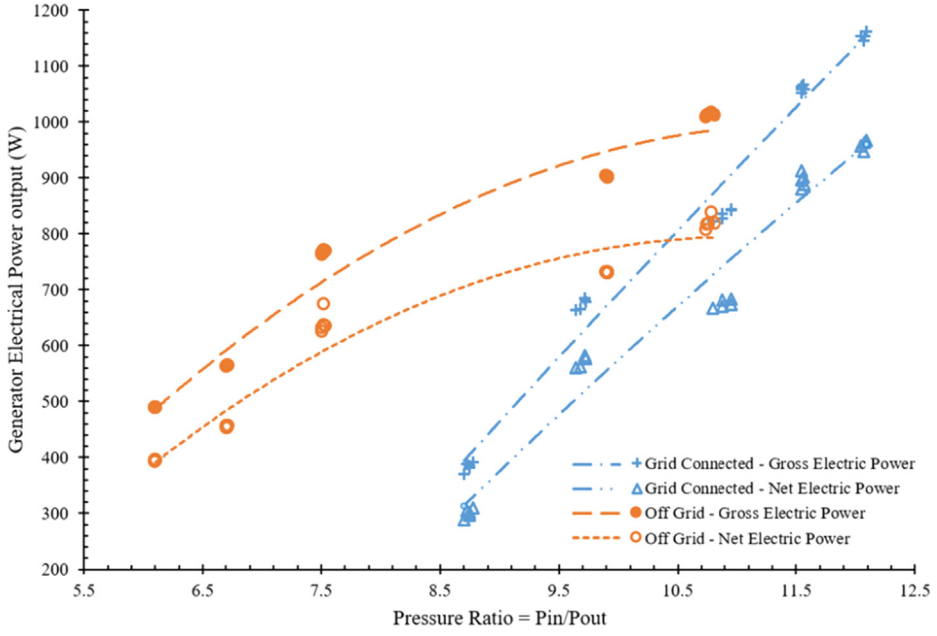

Fig. 5. Generator electrical power output with respect to the pressure ratio.

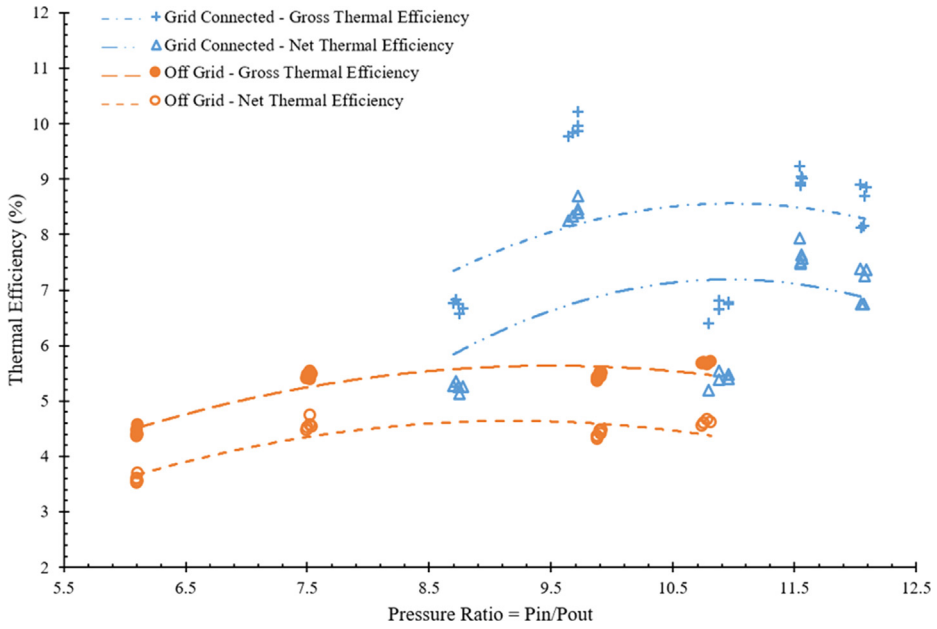

Fig. 6. Thermal Efficiency (gross and net) with respect to pressure ratio.

pressure ratio, but also on the fact that the absolute fluid thermodynamic states (inlet pressure and temperature), along with the expander rotational speed, are of key importance, and these were different for both cases, causing a different overall trend.

Fig. 8 presents the electro-mechanical efficiency as calculated with Eq. (7) in both the grid-connected and off-grid operation. It was not possible to detail and comment on the mechanical and electrical conversion efficiencies separately due to equipment limitation (Torque was not mechanically measured at expander output). The authors followed a lumped parameter technique to combine mechanical and electrical losses together. Similar technique was already presented by Pan et al [40] where transmission and electrical efficiency was lumped in a single parameter. The electro-mechanical efficiency accounts for the mechanical/frictional losses in the expander bearings, coupling and generator, along with the electrical losses in the generator and power electronics summed up together. In other words, the losses which do not contribute the enthalpy reduction (bearing losses and coupling losses, electrical losses) are also included to define electro-mechanical efficiency term.

In general, it can be concluded that the electro-mechanical efficiency of the grid-connected system was higher which contributes to a larger gross power output and higher thermal efficiency in the grid-connected mode. The trends are mainly dependent on the optimal component matching.

Therefore, another important aspect of ORC technology is highlighted: components are often off-the-shelf and integrated to operate together as a system, especially in small-scale systems. It is a common practice not to oversize the components (e.g., expander, generator and

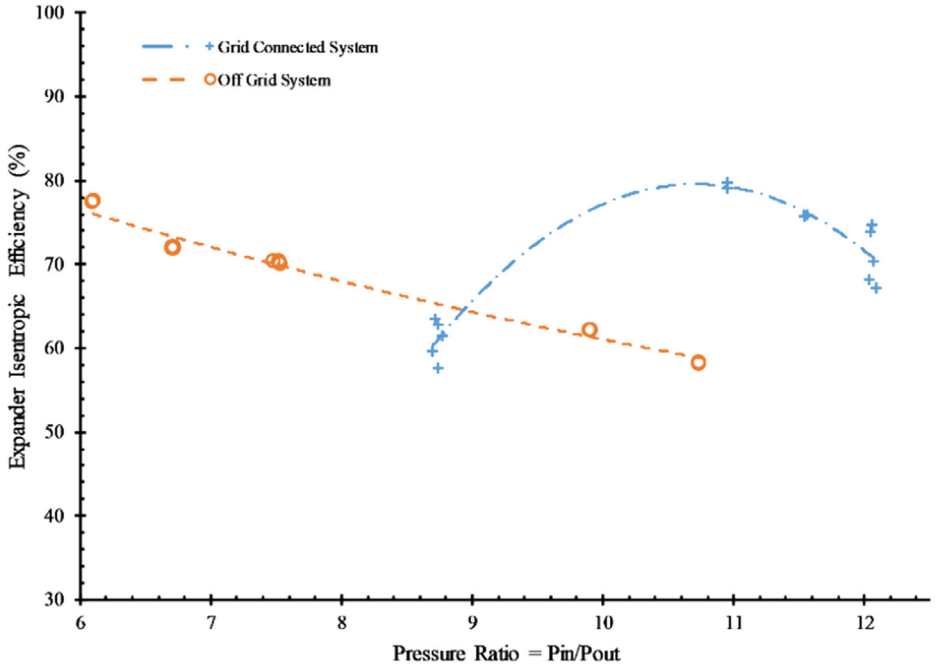

Fig. 7. Expander isentropic efficiency vs. pressure ratio.

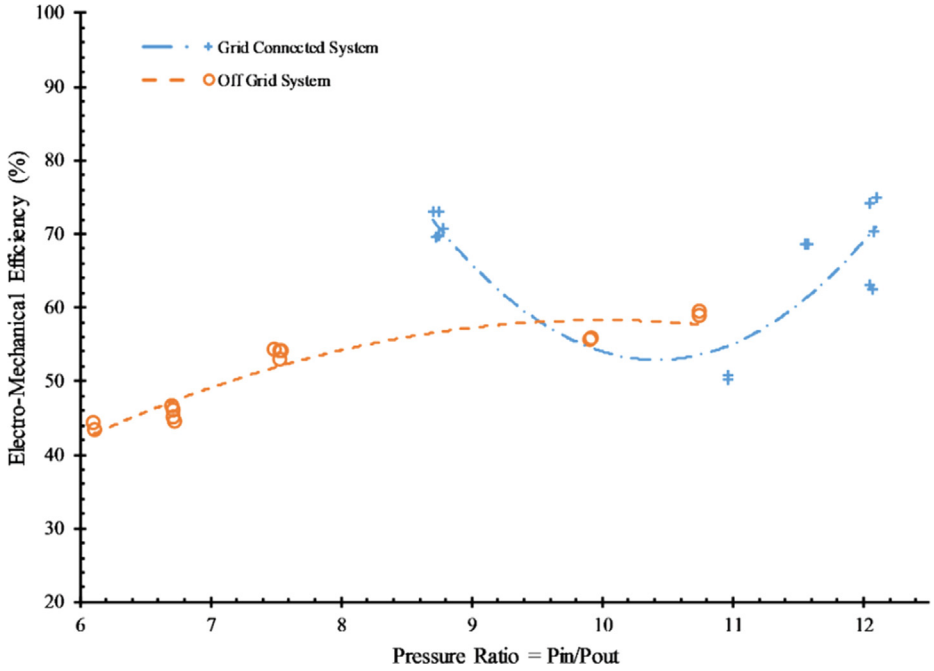

Fig. 8. Electro-Mechanical Efficiency vs pressure ratio.

power electronics) to avoid additional capital costs, but the investigation in Ref. [3] found that expanders are often operated with lower effectiveness when operating at maximum power output for their size. The same needs to be investigated for generators and other equipment of the ORC system such as pumps.

Fig. 9 presents how well the fluid work potential has been converted to consumable electrical power for both systems. The parameter is essentially the product of isentropic efficiency and electro-mechanical efficiency as defined by Eq. (8). It represents how well the energy has been transformed from fluid to electrical power considering the expander-generator system as a whole. The trend is dependent on the component performance in a range of operating conditions. It can be observed that overall the grid-connected system had a better fluid to electric power conversion efficiency due to better compatibility at operational points. Primarily the electro-mechanical losses were lower as compared to the off-grid system, and the grid-connected system was combined with isentropic efficiency peaks resulting in a more suitable system.

Fig. 10 represents the measured electrical pumping power and back work ratio as defined by Eq. (9) with respect to the imposed pressure ratio for a grid-connected and an off-grid system configuration. The back work ratio for the grid-connected system decreased at a larger pressure ratio as the electrical power conversion efficiency increased at higher pressure ratios for the grid-connected system.

The back work ratio trend remained fairly unchanged, and the minor dip in the centre around pressure ratio 8.6 is due to increased

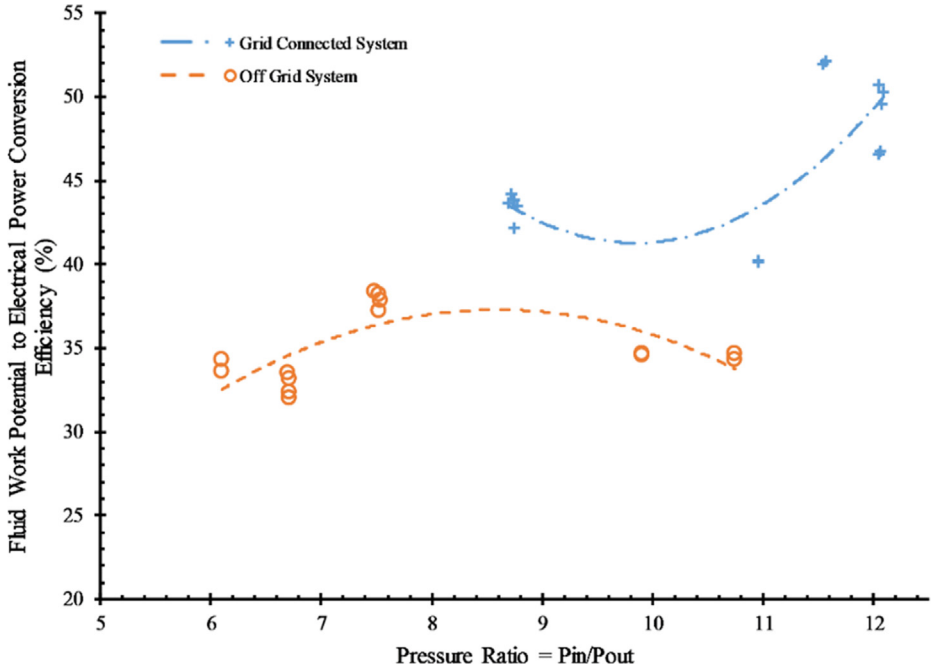

Fig. 9. Percentage of fluid work potential converted to useable electrical power with respect to pressure ratio.

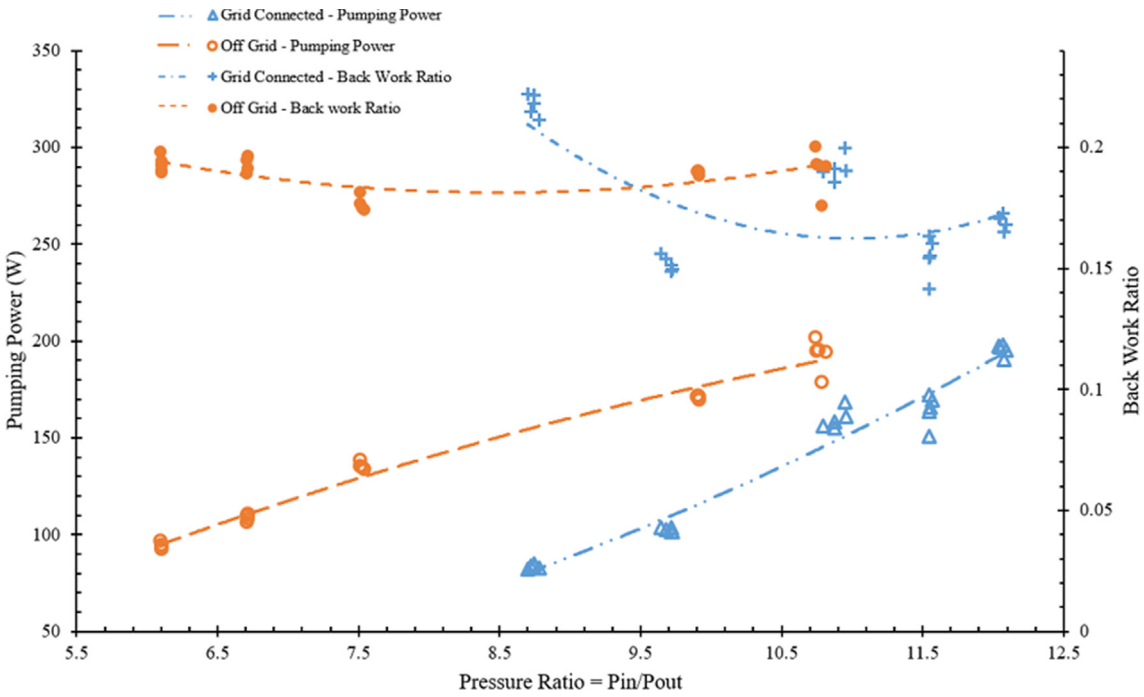

Fig. 10. Pumping power and back work ratio with respect to the pressure ratio.

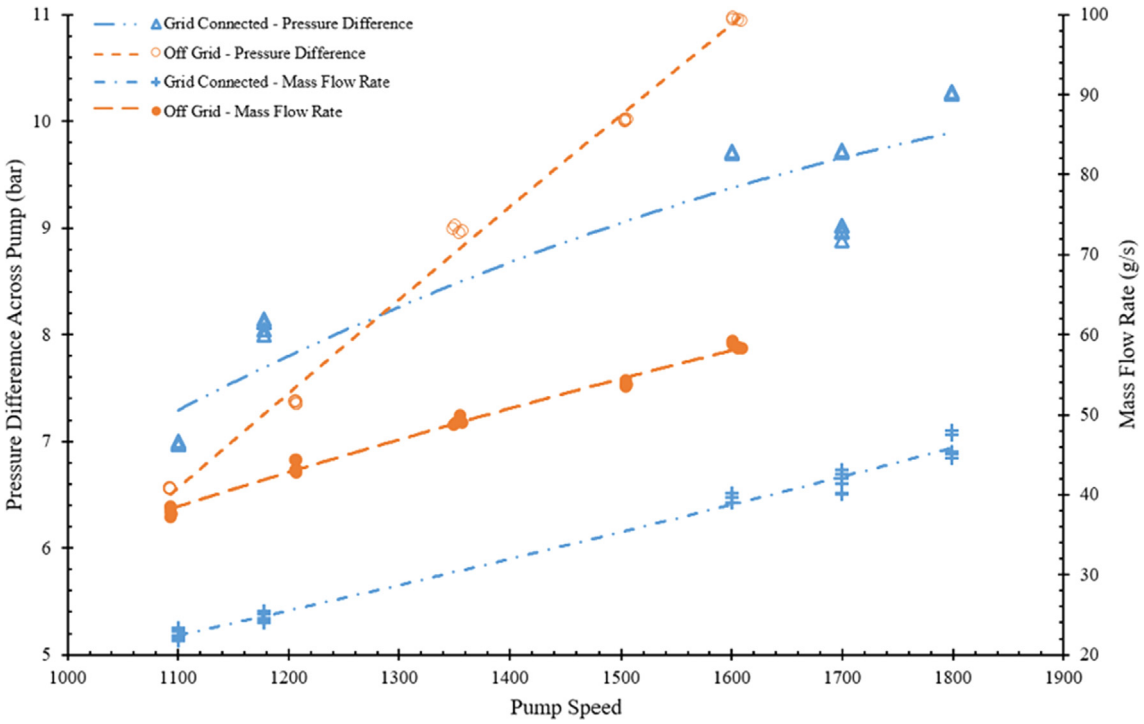

Fig. 11. Pressure difference and mass flow rate with respect to pump speed.

electric power conversion efficiency as observed in Fig. 9. In general, it can be concluded that pumping power increased linearly with the pressure ratio; however, the back work ratio was mainly impacted by the power output characteristics at the expander end. The pumping power for the off-grid system was higher as compared with the grid-connected system, primarily because the larger flow rate was moved in the case of the off-grid system.

Fig. 11 presents the change in the pressure difference across the pump and the imposed mass flow rate for off-grid and grid-connected operation. The pump speed and mass flow rate present a linear response and highlight that the volumetric pump was capable of performing even at the higher pressure ratios without significant leakage losses, as the mass flow rate remains fairly linear with the pump rotational speed. The pressure difference across the pump is also increasing with the pump speed, but it must be noted that the discharge side pressure is not only dependent on the pump, but also on the choking conditions caused by the swept volume and rotational speed of the expander. A larger pressure difference was generated along with a larger mass flow rate off-grid operation for the same pump speed, at the same speed if compared with the grid-connected system. The cause can be associated

Table 4
Uncertainty in the calculated parameters.

Calculated Parameters	Max Uncertainty
Isentropic efficiency of expander, η_{isc}	± 0.87%
Heat input to the evaporator, $\dot{Q}_{in}$	± 1.07 °C
Net power output, $\dot{W}_{net}$	± 1.21%
Work output of expander, $\dot{W}_{exp}$	± 0.97%
Work input to the pump, $\dot{W}_{pu}$	± 0.89%
Gross thermal efficiency, η_{th}	± 1.58%
Net thermal efficiency, η_{net}	± 1.67%
Electro-mechanical efficiency, η_{em}	± 1.56%
Fluid work potential to electrical conversion efficiency, η_{fec}	± 1.63%
Pressure ratio, Pin/Pout	± 1.4%
Back work ratio, *BWR*	± 1.23%

with slightly higher condensing pressure in off-grid operation, which led to a slightly higher net positive suction head available (NPSHA) for the pump, while the lower NPSHA may have contributed to bubble formation and cavitation, thus deteriorating the pump performance. However, further investigation is required to ensure the hypothesis, and the current data are not sufficient to conclude the causes of these observations.

The cost of the retrofitting in the above-discussed work was below 3000USD at the time of implementation and includes the replacement of all equipment (motor/generator, magnetic coupling, regenerative variable frequency drive, power transducer and current transducers) and the installation labour.

4. Uncertainty analysis

The uncertainties were processed with the Engineering Equation Solver software. The measurement-related absolute error ε of a derived quantity Z from the partial derivatives with respect to all involved measurements X_i and their respective uncertainties ε_{Xi} was calculated as follows:

$$\varepsilon_Z = \sqrt{\sum_i \left(\frac{\partial Z}{\partial X_i}\right)^2 (\varepsilon_{Xi})^2} \tag{10}$$

The isentropic efficiency of expander, η_{isc}, heat input to the evaporator, $\dot{Q}_{in}$, the net power output, $\dot{W}_{net}$, work output of expander, $\dot{W}_{exp}$, work input to the pump, $\dot{W}_{pu}$, gross thermal efficiency, η_{th}, net thermal efficiency, η_{net}, electro-mechanical efficiency, η_{em}, fluid work potential to electrical conversion efficiency, η_{fec}, and back work ratio, *BWR*, were calculated from the measures values of the mass flow rate of the working fluid, and enthalpy of the working fluid. The enthalpy of the working fluid is estimated based on the measured values of the temperature and pressure. The results of the uncertainty analysis are provided in Table 4.

5. Conclusions

The retrofitting and performance comparison of a micro-scale organic Rankine cycle test rig in off-grid mode and grid-connected mode is investigated in the present study. The experiments were performed in off-grid operation mode with a self-excited alternating current generator. For the experiments in grid-connected mode, the alternating current generator is replaced with the induction motor, regenerative variable frequency drive and finally connected with a grid. The off-grid organic Rankine cycle system is converted to operate in the grid-connected mode with the ability to operate the expander at speeds independent of the grid line frequency. It is observed that the organic Rankine cycle system can be converted from the off-grid mode to grid-connected mode and can provide higher power, if the component matching is optimal. The following conclusions can be made from the work:

- The grid-connected system is able to supply a larger gross and net electric power to the grid due to better electro-mechanical efficiency and overall better equipment matching with the organic Rankine cycle performance curve. The system is able to supply a maximum electric power of 1.162 kW and net electric power of 0.967 kW in grid-connected mode, while the off-grid maximums are 1.016 kW gross and 0.838 kW net electric power.
- The electro-mechanical conversion losses are lower in grid-connected operation compared to off-grid operation mode.
- The difference in the electro-mechanical conversion losses emphasises the need for advanced modelling to derive off-design performance and the optimum component-matching requirement when selecting off-the-shelf items for the micro organic Rankine cycle system.
- The thermal efficiency (both gross and net) is higher in grid-connected operation as the electro-mechanical efficiency is higher. Also the expander isentropic efficiency is improved as the whole organic Rankine cycle performance curve has shifted and a higher pressure ratio could be imposed without exceeding maximum pressure limits in the evaporator.
- The possibility of the presence of non-condensable gasses can contribute to the deterioration of the performance of the organic Rankine cycle system.
- The regenerative variable frequency drive with an induction motor allows operation of the expander initially as a pump and then switches to expander mode smoothly; also the control of expander speed allows an additional and significant control parameter for operational control optimisation of the organic Rankine cycle performance.

For future research, the present results will be extended to investigate the dynamic performance and control of the grid-connected and off-grid organic Rankine cycle systems.

Declaration of Competing Interest

The authors declare that they have no known competing financial interests or personal relationships that could have appeared to influence the work reported in this paper.

Acknowledgement

The research presented in this paper has received funding from the European Union's Horizon 2020 research and innovation programme with two Marie Skłodowska-Curie Fellowships under grant agreement number 844023 (project SuperVGE) and 751947 (project DYNCON-ORC), respectively. The infrastructure and experimental works were supported under the framework of the Research and Development Program of the Korea Institute of Energy Research (B9-2451-6).

Appendix A. Supplementary material

Supplementary data to this article can be found online at https://doi.org/10.1016/j.applthermaleng.2020.115889.

References

[1] UNFCCC. Conference of the Parties (COP), Paris Climate Change Conference-November 2015, COP 21. Adopt Paris Agreement Propos by Pres, vol. 21932, 2015, pp. 32. doi: FCCC/CP/2015/L.9/Rev.1.
[2] European Commission, 2020 climate & Energy Package n.d. https://ec.europa.eu/clima/policies/strategies/2020_en (accessed June 11, 2018).
[3] B.-S. Park, M. Usman, M. Imran, A. Pesyridis, Review of Organic Rankine Cycle experimental data trends, Energy Convers Manag 173 (2018) 679–691, https://doi.org/10.1016/J.ENCONMAN.2018.07.097.

[4] S. Lion, C.N. Michos, I. Vlaskos, C. Rouaud, R. Taccani, A review of waste heat recovery and Organic Rankine Cycles (ORC) in on-off highway vehicle Heavy Duty Diesel Engine applications, Renew. Sustain. Energy Rev. 79 (2017) 691–708, https://doi.org/10.1016/j.rser.2017.05.082.

[5] J. Larjola, Electricity from industrial waste heat using high-speed organic Rankine cycle (ORC), Int. J. Prod. Econ. 41 (1995) 227–235, https://doi.org/10.1016/0925-5273(94)00098-0.

[6] F. Campana, M. Bianchi, L. Branchini, A. De Pascale, A. Peretto, M. Baresi, et al., ORC waste heat recovery in European energy intensive industries: Energy and GHG savings, Energy Convers Manag 76 (2013) 244–252, https://doi.org/10.1016/j.enconman.2013.07.041.

[7] P. Colonna, E. Casati, C. Trapp, T. Mathijssen, J. Larjola, T. Turunen-Saaresti, et al., Organic Rankine cycle power systems: from the concept to current technology, applications and an outlook to the future, J. Eng. Gas Turbines Power 137 (2015) 1–19, https://doi.org/10.1115/1.4029884.

[8] V. Pethurajan, S. Sivan, G.C. Joy, Issues, comparisons, turbine selections and applications – An overview in organic Rankine cycle, Energy Convers. Manag. 166 (2018) 474–488, https://doi.org/10.1016/j.enconman.2018.04.058.

[9] T.C. Hung, T.Y. Shai, S.K. Wang, A review of organic rankine cycles (ORCs) for the recovery of low-grade waste heat, Energy 22 (1997) 661–667, https://doi.org/10.1016/S0360-5442(96)00165-X.

[10] S. Lecompte, H. Huisseune, M. van den Broek, B. Vanslambrouck, M. De Paepe, Review of organic Rankine cycle (ORC) architectures for waste heat recovery, Renew. Sustain. Energy Rev. 47 (2015) 448–461, https://doi.org/10.1016/j.rser.2015.03.089.

[11] E. Wang, Z. Yu, P. Collings, Dynamic control strategy of a distillation system for a composition-adjustable organic Rankine cycle, Energy 141 (2017) 1038–1051, https://doi.org/10.1016/j.energy.2017.09.141.

[12] G. Cavazzini, P. Dal Toso, Techno-economic feasibility study of the integration of a commercial small-scale ORC in a real case study, Energy Convers Manag 99 (2015) 161–175, https://doi.org/10.1016/j.enconman.2015.04.043.

[13] M. Imran, F. Haglind, M. Asim, A.J. Zeb, Recent research trends in organic Rankine cycle technology: A bibliometric approach, Renew. Sustain. Energy Rev. 81 (2018) 552–562, https://doi.org/10.1016/j.rser.2017.08.028.

[14] D. Walraven, B. Laenen, W. D'haeseleer, Comparison of thermodynamic cycles for power production from low-temperature geothermal heat sources, Energy Convers Manag 66 (2013) 220–233, https://doi.org/10.1016/j.enconman.2012.10.003.

[15] B. Saleh, G. Koglbauer, M. Wendland, J. Fischer, Working fluids for low-temperature organic Rankine cycles, Energy 32 (2007) 1210–1221, https://doi.org/10.1016/J.ENERGY.2006.07.001.

[16] J. Xu, C. Yu, Critical temperature criterion for selection of working fluids for subcritical pressure Organic Rankine cycles, Energy 74 (2014) 719–733, https://doi.org/10.1016/j.energy.2014.07.038.

[17] M. Usman, M. Imran, Y. Yang, D.H. Lee, B.-S. Park, Thermo-economic comparison of air-cooled and cooling tower based Organic Rankine Cycle (ORC) with R245fa and R1233zde as candidate working fluids for different geographical climate conditions, Energy 123 (2017) 353–366, https://doi.org/10.1016/J.ENERGY.2017.01.134.

[18] F. Alshammari, M. Usman, A. Pesyridis, Expanders for organic Rankine cycle technology, in: E. Wang (Ed.), Org. Rank. Cycle Technol. Heat Recover., IntechOpen, Rijeka, 2018. doi: 10.5772/intechopen.78720.

[19] F. Alshammari, A. Karvountzis-Kontakiotis, A. Pesyridis, M. Usman, Expander technologies for automotive engine organic Rankine cycle applications, Energies 11 (2018) 1905, https://doi.org/10.3390/EN11071905.

[20] M. Imran, M. Usman, D.H. Lee, B.S. Park, Volumetric expanders for low grade & waste heat recovery applications, Renew. Sustain. Energy Rev. 57 (2016) 1090–1109, https://doi.org/10.1016/j.rser.2015.12.139.

[21] G. Qiu, H. Liu, S. Riffat, Expanders for micro-CHP systems with organic Rankine cycle, Appl. Therm. Eng. 31 (2011) 3301–3307, https://doi.org/10.1016/j.applthermaleng.2011.06.008.

[22] Z. Gnutek, P. Kolasiński, The application of rotary vane expanders in organic Rankine cycle systems—thermodynamic description and experimental results, J. Eng. Gas Turbines Power 135 (2013) 061901, , https://doi.org/10.1115/1.4023534.

[23] J.C. Chang, T.C. Hung, Y.L. He, W. Zhang, Experimental study on low-temperature organic Rankine cycle utilizing scroll type expander, Appl. Energy 155 (2015) 150–159, https://doi.org/10.1016/j.apenergy.2015.05.118.

[24] S. Declaye, S. Quoilin, L. Guillaume, V. Lemort, Experimental study on an open-drive scroll expander integrated into an ORC (Organic Rankine Cycle) system with R245fa as working fluid, Energy 55 (2013) 173–183, https://doi.org/10.1016/j.energy.2013.04.003.

[25] G. Pei, J. Li, Y. Li, D. Wang, J. Ji, Construction and dynamic test of a small-scale organic Rankine cycle, Energy 36 (2011) 3215–3223, https://doi.org/10.1016/j.energy.2011.03.010.

[26] Z. Miao, J. Xu, X. Yang, J. Zou, Operation and performance of a low temperature organic Rankine cycle, Appl. Therm. Eng. 75 (2015) 1065–1075, https://doi.org/10.1016/j.applthermaleng.2014.10.065.

[27] M. Farrokhi, S.H. Noie, A.A. Akbarzadeh, Preliminary experimental investigation of a natural gas-fired ORC-based micro-CHP system for residential buildings, Appl. Therm. Eng. (2013), https://doi.org/10.1016/j.applthermaleng.2013.11.060.

[28] J.L. Wang, L. Zhao, X.D. Wang, An experimental study on the recuperative low temperature solar Rankine cycle using R245fa, Appl. Energy 94 (2012) 34–40, https://doi.org/10.1016/j.apenergy.2012.01.019.

[29] N. Yamada, Y. Tominaga, T. Yoshida, Demonstration of 10-Wp micro organic Rankine cycle generator for low-grade heat recovery, Energy 78 (2014) 806–813, https://doi.org/10.1016/j.energy.2014.10.075.

[30] E. Yun, D. Kim, S.Y. Yoon, K.C. Kim, Experimental investigation of an organic Rankine cycle with multiple expanders used in parallel, Appl. Energy 145 (2015) 246–254, https://doi.org/10.1016/j.apenergy.2015.02.022.

[31] U. Muhammad, M. Imran, D.H. Lee, B.S. Park, Design and experimental investigation of a 1kW organic Rankine cycle system using R245fa as working fluid for low-grade waste heat recovery from steam, Energy Convers. Manag. 103 (2015) 1089–1100, https://doi.org/10.1016/j.enconman.2015.07.045.

[32] M. Usman, M. Imran, D.H. Lee, B.-S. Park, Experimental investigation of off-grid organic Rankine cycle control system adapting sliding pressure strategy under proportional integral with feed-forward and compensator, Appl. Therm. Eng. 110 (2017) 1153–1163, https://doi.org/10.1016/j.applthermaleng.2016.09.021.

[33] A. Landelle, N. Tauveron, P. Haberschill, R. Revellin, S. Colasson, Organic Rankine cycle design and performance comparison based on experimental database, Appl. Energy 204 (2017) 1172–1187, https://doi.org/10.1016/j.apenergy.2017.04.012.

[34] Y. Feng, T.-C. Hung, T.-Y. Su, S. Wang, Q. Wang, S.-C. Yang, et al., Experimental investigation of a R245fa-based organic Rankine cycle adapting two operation strategies: Stand alone and grid connect, Energy 141 (2017) 1239–1253, https://doi.org/10.1016/J.ENERGY.2017.09.119.

[35] A. Hughes, B. Drury, Induction Motors – Rotating Field, Slip and Torque, Electr. Mot. Drives, Newnes (2013) 141–167, https://doi.org/10.1016/B978-0-08-098332-5.00005-X.

[36] M.O. Mclinden, E.W. Lemmon, M.L. Huber, The Refprop database for the thermophysical, in: Int. Congr. Refrig., Washington D.C., 2003, p. 1–8.

[37] V. Lemort, S. Quoilin, S. Declaye, A. Zoughaib, L. De Thermodynamique, Dynamic modelling and optimized model predictive control strategies for the ORC, in: First Int Semin ORC Power Syst, 2011, pp. 1–24.

[38] J.-F. Oudkerk, S. Quoilin, S. Declaye, L. Guillaume, E. Winandy, V. Lemort, Evaluation of the energy performance of an organic Rankine cycle-based micro combined heat and power system involving a hermetic scroll expander, J. Eng. Gas Turbines Power 135 (2013) 042306, , https://doi.org/10.1115/1.4023116.

[39] Y. Qiang Feng, T.C. Hung, T.Y. Su, S. Wang, Q. Wang, S.C. Yang, Experimental investigation of a R245fa-based organic Rankine cycle adapting two operation strategies: Stand alone and grid connect, Energy 141 (2017) 1239–1253, https://doi.org/10.1016/j.energy.2017.09.119.

[40] L. Pan, H. Wang, W. Shi, Regulation law of turbine and generator in organic Rankine cycle power generation experimental system, Trans. Tianjin Univ. 20 (2014), https://doi.org/10.1007/s12209-014-2220-z.